ADVANCED MATERIALS INTERFACES
Open Access
www.advmatinterfaces.de

Titanium Oxysulfate-Derived 1D Lepidocrocite Titanate Nanostructures

Sukanya Maity, Mohamed Ibrahim, Hussein Badr, Treesa Reji, Mary Q. Hassig, Tongjie Zhang, Christopher Li, Johanna Rosén,* and Michel W. Barsoum**

Nanostructured titania, TiO_2, holds significant importance in various scientific fields and technologies for their distinctive properties and multipurpose characteristics. In this article, the facile, economical, and scalable synthesis of 1D lepidocrocite, 1DL, titania nanostructures derived from a water-soluble Ti precursor, titanium oxysulfate (with oxidation of Ti^{+4}) at temperature <100 °C under atmospheric pressure is discussed. Titanium oxysulfate with tetramethyl ammonium hydroxide, TMAH, is simply reacted to yield individual lepidocrocite titania-based chain-forming nanofilaments, NFs, 6×6 Å^2 in minimal cross-section and aspect ratios of ≈20 1DLs. If only ethanol is used for washing, the 1DL self-assemble into ≈10 µm, porous mesostructured particles, PMPs. If water is used, quasi-2D sheets form instead. Characterization of the resulting powders showed them to be quite similar to those derived from TiB_2, and other water-insoluble Ti precursors. The 1DL bandgap energies are ≈4 eV, due to quantum confinement. They adsorbed rhodamine 6G. The latter also sensitized the 1DLs and allowed for dye degradation using only visible light. Used as electrodes in supercapacitors, the 1DLs can be cycled over 1.6 V and result in high power densities (300 W kg^{-1}). Stronger birefringence started to appear in samples with concentrations >15 gL^{-1} indicating the formation of a liquid crystal phase. This new synthesis protocol enables the cheaper scalable production of 1DLs with significant implications across various fields.

1. Introduction

Titania, TiO_2, nanostructures have been, and remain, of great research interest because of their physical properties and chemical structures. Their wide range of potential applications, such as paint pigment, gas sensors, solar and fuel cells, energy storage, catalysis, photoluminescence, and photocatalysis, render them of significant research and industrial relevance.[1–3] 1D and 2D materials have unique properties compared to their 3D counterparts, importantly in terms of the higher specific surface areas, SSAs, electronic properties, and if small enough quantum confinement.[4,5] Commercially available TiO_2 nanostructure, that is, P25, stands out for its exceptional photocatalytic activity and is considered the gold standard for catalytic applications. However, its relatively expensive synthesis process (flame pyrolysis) is one of its major drawbacks.[6–8] P25 is also not stable for extended times in water.[9]

Titania nanoparticles can be derived from Ti sulfate precursors using several methods, such as sol-gel, hydrothermal, precipitation, microwave-, ultrasonic-assisted synthesis, etc.[10–13] The sol-gel and precipitation methods are relatively simple and do not require sophisticated instruments but may result in lower control over particle size and high chance of impurity compared to hydrothermal and microwave-assisted synthesis. However, hydrothermal and microwave or ultrasonic-assisted synthesis results in the rapid, uniform synthesis of nanoparticles but requires specialized reactors and equipment, which makes them expensive to synthesize. Lithium titanate microparticles were synthesized from titanium oxysulfate via several hydrothermal-calcination processes by Hong et al. and applied as anode material for Li-ion batteries.[14] Further, Xiao et al. and Szilágyi et al. used the chemical treatment of Ti sulfate with H_2O_2 to produce thin titania films[15] and titanium dioxide precipitates,[16] respectively.

In 2022 we reported on a simple, facile, scalable, low-cost, one-pot, solution-precipitation scheme to produce a number of nanostructured oxides.[17] The method entails reacting various precursor powders in tetramethylammonium

S. Maity, J. Rosén
Department of Physics
Chemistry and Biology (IFM)
Linköping University
Linköping 58183, Sweden
E-mail: sukanya.maity@liu.se; johanna.rosen@liu.se
M. Ibrahim, H. Badr, T. Reji, M. Q. Hassig, T. Zhang, C. Li, M. W. Barsoum
Department of Materials Science and Engineering
Drexel University
Philadelphia, PA 19104, USA
E-mail: barsoumw@drexel.edu

The ORCID identification number(s) for the author(s) of this article can be found under https://doi.org/10.1002/admi.202400866

DOI: 10.1002/admi.202400866

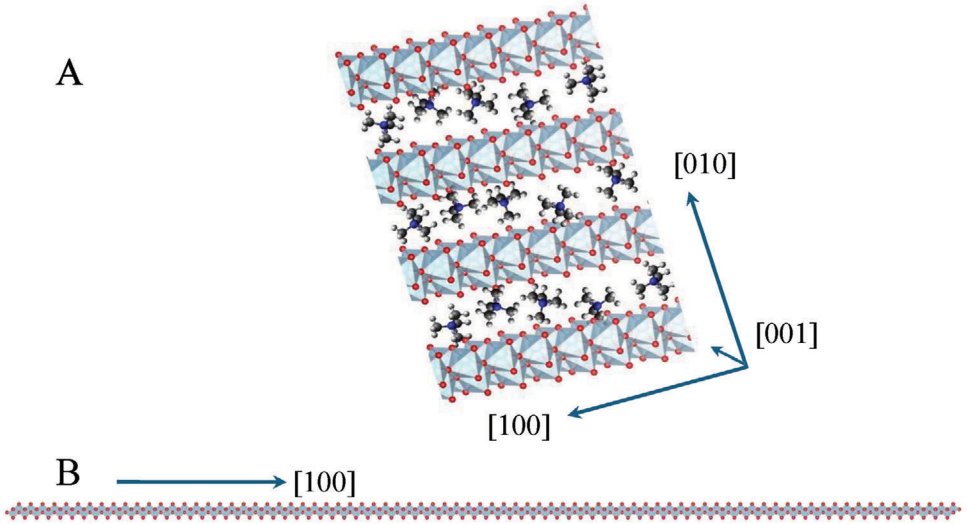

Figure 1. Schematic of, A) isometric view of 1DL intercalated with TMA+. Water of hydration is not shown for clarity's sake.; B) Typical aspect ratio of one strand (drawn to scale). 1DLs grow along *a- or* [100] direction and stack along *b*- or [010]. Width is along c- or [001]. The smallest width is 2 TiO_6 octahedra wide. Minimal final cross-section of 2 × 2 edges shared TiO_6 octahedra.

hydroxide (TMAH) aqueous solutions at temperatures <100 °C, under ambient pressures. In one case, several Mn-containing precursor powders (e.g., Mn_3O_4, Mn_3O_2, MnB, etc.) were reacted with TMAH aqueous solution in the 50–85 °C temperature range for several days.[18,19] The resultant 2D birnessite sheets ≈2 ± 0.4 nm thick, were remarkably crystalline and demonstrated electrochemical activity toward O_2 electrocatalysis and supercapacitor applications.[20,21] In another study, we reacted Fe-containing compounds with TMAH and other alkali aqueous solutions to synthesize Fe_3O_4 nanoparticles.[22]

More germane to this work is the reaction of more than a dozen Ti-containing insoluble precursors (e.g., TiC, TiN, TiB_2, etc.) – with Ti oxidation states <4 – with TMAH. Here again, the reaction conditions were <100 °C for tens of hours, h, at 1 atm. In this case, the end result was 1D lepidocrocite titanate-based nanofilaments, NFs, henceforth referred to as 1DLs sketched in **Figure 1**. The NFs grow along the [100] direction and stack along the [010] direction (Figure 1A). Their minimal cross-section was determined to be in the 6 × 6 Å^2 range.[23–27] If the 1DLs in one gram are stacked, end to end, they would span ≈600 million kilometers. It is important to note here that there are many literature claims for the formation of 1D titania.[28] However, as far as we are aware, none fulfill the quantum definition of 1D, wherein quantum confinement is observed. In sharp contradistinction to all other claims of 1D titania, our 1DL's bandgap energy, E_g, is ≈4 eV, which is a record for a titania-based material. This enhancement in E_g is strong, albeit indirect, evidence for our extreme dimensions.

Using several characterization techniques, including X-ray diffraction, XRD, Raman spectroscopy, and high-resolution transmission electron microscopes (HRTEM), we now have a decent understanding of the 1DL structure. The latter is that of lepidocrocite, which grows in the *a*-direction and stacks in the *b*-direction (Figure 1A). Remarkably, the minimum cross-section is 2 × 2 edge-sharing TiO_6 octahedra in the *b* and *c*-directions. Based on HRTEM images we established that typical 1DLs are 10–50 nm long. Figure 1B sketches, to scale, a typical 30 nm long snippet. The main takeaway here is the extreme aspect ratio from which much evolves.[23,24,26] These relatively short snippets can be described in several ways. The simplest is as linear polymer chains with a $[Ti_{15}O_{32}]_n{}^{4-}$ chemistry, and n values that depend on their lengths. At 30 nm, n is ≈10 (Figure 1B). These short chains self-assemble into larger elementary fibrils, or protofibrils, that self-assemble into microfibrils that, in turn, self-assemble into fibers, with lengths on the micrometer scale. Using fibrils in our context is deliberate to make the connection between our work and cellulose. In cellulose short polymer chains, $[C_6H_{10}O_5]_n$, self-assemble into protofibrils that grow in microfibrils, etc.[29]

Figure 2 summarizes our process in which plastic bottles are used as reaction vessels that are heated to various temperatures under 1 atm pressure. In previous work, using TiB_2 as our Ti-precursor, the reaction is complete in tens of hours, after which the reaction mixture is washed with ethanol to pH ≈7 (Figure 2B). What happens next depends critically on post-processing. If the ethanol is simply allowed to evaporate, the 1DLs self-assemble into porous mesostructured particles, or PMPs (Figure 2F). At that stage, TMA cations are intercalated between the NFs (Figure 2G).

If, after reaching a pH of 7, the ethanol is exchanged with water (Figure 2C), a highly stable transparent colloid is formed that, when filtered, results in self-standing films comprised of quasi, or pseudo, 2D flakes (Figure 2D). The latter are labeled quasi, q-2D because, as shown below, they are comprised of jumbled, overlapping fibrils, not unlike a plate of spaghetti.

Our 1DL nanofibers consistently outperformed commercial anatase, P25, in various applications. In photocatalytic water splitting, the 1DL nanofibers achieved an apparent quantum yield of 11.7% and remained stable in aqueous environments for over six months, including 300 h of continuous illumination.[30] For dye degradation, these nanofilaments enabled the

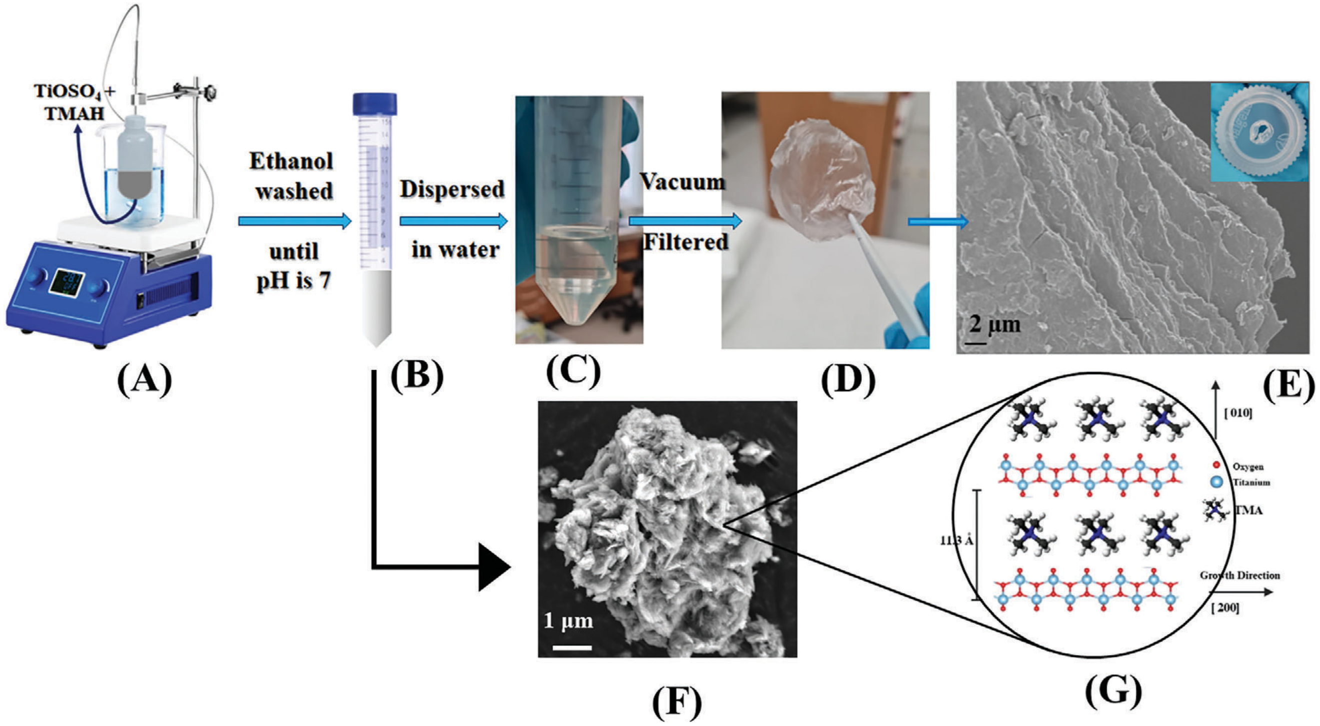

Figure 2. Schematic of bottom-up synthesis route to produce 1DLs starting with $TiOSO_4$ and TMAH, A) using a hot plate and stirrer. B) Ethanol washes to pH 7. C) The addition of water leads to a transparent suspension D) when filtered yields a transparent white film. E) SEM micrograph showing pseudo-2D character of 1DLs. F) To prepare PMPs, the washed solid is directly dried without adding water.

photodegradation of dyes within the visible spectrum, a task at which P25 was ineffective.[9] The 1DL-based nanomaterials used in water purification absorbed up to 424 mg of uranium (U^{4+}) per gram of 1DL, effectively converting contaminated water into potable water.[31] In the field of energy storage, electrodes made from these 1DL nanofibers demonstrated robust performance in both lithium-ion and lithium-sulfur systems.[27] Moreover, composites incorporating our 1DLs with a dynamic covalent thiol-yne network showed significant improvements in mechanical properties, resulting in a 500-fold increase in the modulus at 60 wt% filler when compared to the neat polymer.[17]

Somewhat surprisingly, 1DL production is quite simple: we react earth abundant non-toxic, Ti-containing precursors, such as TiC or TiB_2, with TMAOH for tens of hours at temperatures <100 °C and ambient pressures (Figure 2A). It is during the reaction stage that the short chains form. In our work to date, the Ti-precursors were insoluble Ti-compounds on the hypothesis that a solid/liquid interface was needed for 1DL nucleation. And while we obtained effective results with TiB_2,[26] the questions posed were: Can water soluble and cheaper precursors be used? If such salts are used, will the conversion to 1DLs be faster? Herein we show that the answer to all questions is yes.

In this work, we start with $TiOSO_4$, an inexpensive, water-soluble, Ti-salt, and react it with TMAH in the 60–95 °C temperature range for times ranging from 3 hours, h, to 5 days, d (see **Table 1**). We also explored the effect of the Ti:TMAH molar ratio, R, on the final products and kinetics. Lastly, we characterized the reaction products and showed them all to be 1DL. This method transcends the limitations of our previous approaches, leveraging a solution precipitation process fine-tuned for lower temperatures and minimal reagent use. It results in a faster kinetics, cost-effective, time-efficient, and scalable approach perfect for industrial applications. The syntheses and characterizations were carried out in two labs: One in Sweden (Lab 1) and one in the USA (Lab 2). Table 1 summarizes the runs carried out. In Lab 2, R was fixed at 0.2.

Table 1. Summary of runs carried out in this work. The Ti:TMAH molar ratio, R, in lab 2 was set at 0.2. The other runs were carried out in Lab 1, with various R values.

Molar ratio [Ti:TMAH]	Temperature [°C]	Time [h/day]	TMAH Concentration [wt%]	Lab
0.2	80	3 h	25	2
0.2	80	12 h	25	2
0.2	80	22 h	25	2
0.2	95	3 h	25	2
0.2	95	12 h	25	2
0.2	95	22 h	25	2
0.2	80	2 d	25	1
0.3	60	3 d	20	1
0.5	70	4 d	15	1
0.2	80	5 d	10	1
0.6	80	5 d	25	1

2. Experimental Section

Materials: Lab 1: Titanium (IV) oxysulfate, $TiOSO_4$ (≥ 29% wt% Ti, anhydrous basis, powder) and TMAH (25 wt%), potassium hydroxide (KOH), polytetrafluoroethylene (PTFE) were procured commercially (Sigma Aldrich). Polyvinylidene (PVDF), carbon black, and N-methyl-2-pyrrolidone (NMP) were also procured commercially (ThermoFisher Scientific). Ethanol, EtOH, 200 proof, and sulfuric acid, H_2SO_4, were obtained from VWR Chemicals. Lithium sulfate (Li_2SO_4) and sodium sulfate (Na_2SO_4) were procured from Alfa Aesar.

Lab 2: The $TiOSO_4$ was procured commercially (Thomas Scientific ≥29% wt% Ti) and TMAH was purchased from Alfa Aesar (25 wt% in DI water, 99.9999%). Ethanol, EtOH, 200 proof.

The major variable explored by Lab 1 was the TMAH/1DL ratio or R-value. In lab 2, R was fixed at 0.2 and the main variables were the reaction times and temperatures (Table 1).

Experimental Details: A schematic of the one-pot, method to make 1DLs is shown in Figure 2. In short, the reactants were mixed in plastic bottles that were then heated to various temperatures for predetermined times (Figure 2A). As just noted, a summary of runs carried out herein are listed in Table 1. The experimental techniques in Lab 1 and 2 were slightly different and are described below separately.

Lab 1: The synthesis involves mixing the $TiOSO_4$ powder in the TMAH solution in R values that ranged from 0.22 to 0.6 at temperatures that ranged from 60–80 °C. First, $TiOSO_4$, in powder form, was added to the TMAH solution in polyethylene bottles into which a hole was poked (inset in Figure 2E) to prevent any pressure buildup. The system was kept on a magnetic stirrer in an oil bath for 2 d or more (Table 1).

When the $TiOSO_4$ dissolved in the TMAH a clear solution was obtained. After the reaction, a white sediment (Figure 2B) was obtained that was in turn washed with EtOH several times until the pH was ≈7 (Figure 2B) and then centrifuged at 2500 rpm until the supernatant was clear. After discarding the supernatant, the precipitate was dispersed in DI *water* and shaken until a clear, transparent colloid was formed at all colloidal concentrations (Figure 2C). The latter was then vacuum filtered to obtain free-standing filtered films, FFs, (Figure 2D,E) that were air dried and characterized.

If the reaction products are washed with EtOH – to remove excess TMA^+ cations – and air dried (i.e., without dispersing in water), spherical, free-flowing, PMPs (Figure 2F) were obtained and characterized. Note that at that stage the TMA^+ cations remain between the 1DLs (Figure 2G).

Lab 2: Samples were prepared by reacting $TiOSO_4$ (Thomas Scientific, 29% Ti) with TMAH (Alfa Aesar, 25 wt% in DI water, 99.9999%) at 80 °C in polyethylene bottles in which two 23G needles were inserted to prevent any pressure buildup. The reactants were stirred using a magnetic stir bar. The Ti:TMAOH mole ratio was kept at 0.2 (Table 1). After reaction, the product was then poured into a 50 mL centrifuge tube, centrifuged (Sorvall ST 16 Langenselbold, Germany) at 3500 RPM for 2 min, and the resulting supernatant was discarded. The remaining solid was washed several times with ethanol until a neutral pH, as indicated by pH strips. Subsequently, the supernatant was discarded, leaving only a white sediment in the tube. Then, water was added, and the material was suspended by vortex shaking resulting in the formation of a highly stable, again transparent, colloid. Upon vacuum filtration, this colloid yielded pseudo 2D free-standing films (Figure 2D). At this juncture, the protocol employed resulted in a final morphology as that obtained in lab 1.

Caution: TMAOH is highly toxic, so all reactions and washing were conducted in a fume hood with caution, using appropriate personal protective equipment (e.g., face shield, safety goggles, lab coats, gloves, etc.) to prevent any skin contact.

Yield: The 1DL reaction yield was calculated by comparing the actual weight of the dried 1DL PMPs obtained after synthesis – assumed to be TiO_2 – to the theoretical yield. Since 1 g of $TiOSO_4$ yields 0.5 g of TiO_2, we assume:

$$\text{Yield} = \frac{Weight\ of\ dried\ 1DL}{0.5\ g\ \frac{Tio2}{1\ gm\ Tioso4}} \tag{1}$$

Prior to the yield calculation, the synthesized powder was heated to 400 °C for 4 h in air to remove water and the TMA cations. This temperature was chosen because TGA results (not shown) indicate there was no more weight loss beyond 400 °C.

Characterization: Lab 1: The structures and crystallinities were analyzed from powder X-ray diffraction, XRD (Panalytical; model: X'pert, Netherlands) patterns. Scans were conducted in the 5 to 80° 2θ range, with a step size of 0.02° and a scan rate of 0.5 s/step. The radiation used was CuK_α (40 kV, 40 mA). The PMPs were washed with ethanol and air-dried in RT before XRD analysis.

The resulting morphologies were imaged in a field emission scanning electron microscope, SEM (Zeiss; Model: Sigma 300, Germany) at varying magnifications. The chemistries of the 2D films and PMPs were qualitatively analyzed using an energy-dispersive X-ray spectroscope (EDS) (Oxford Instruments X-Max, 80 mm^2 equipped with a silicon drift detector) attached to the SEM. The air-dried PMPs were dispersed on carbon tape and sputtered with a carbon coating before SEM analysis. For cross-sectional imaging of FFs, the latter were fractured into small sections and mounted on a sample holder. To view individual 1DLs, a colloidal suspension was diluted to 10^{-6} mg ml^{-1} before drop casting onto a carbon mesh.

A Raman system, integrated with an inverted microscope (Nikon Ti-E, Japan) with a 60× air objective (Nikon, NA = 0.7), was used to obtain Raman spectra. A 532 nm DPSS (diode-pumped solid-state) laser (λ-beam, RGB Photonics, Germany) was used for excitation with the output power set to 5 mW. A spectrograph (Andor Kymera 328i, UK) with a 600 mm^{-1} diffraction grating (blazed at 500 nm) was used for analysis. The signal was collected using an EMCCD camera (Andor Newton DU970P-BVF, UK).

UV–vis spectroscopy (Shimadzu, model: UV-2600, Japan) was used to obtain absorption spectra of the colloids and the PMPs. The latter were dispersed in water (concentration 0.1 mg ml^{-1}) through stirring and poured into quartz cuvettes (Fisher Scientific). This was only done, however, after a background measurement was carried out for the baseline correction to set the blank as the zero-absorption reference. For the 1DL colloid suspension, an appropriate concentration (0.1 mg ml^{-1}) was maintained for accruing spectra according to the instrument's sensitivity range.

For electrochemical measurements, the active material, PMPs, was mixed with PVDF and acetylene black in an 8:1:1 weight ratio and a slurry was prepared with the help of an NMP solution. The slurry was then drop-cast onto a carbon cloth (mass loading of the active material to the carbon cloth is 6.36 mg cm^{-2}). All runs used glassy carbon electrodes (CHI instruments, China) as current collectors and glass microfiber membranes as separators (Whatman, General Electrics, USA). Activated carbon, AC, discs – with 10 wt.% PTFE binder – were used as the counter electrodes. The reference electrodes were Ag/AgCl and Hg/HgO for acidic/neutral and basic electrolyte media, respectively. The fabricated electrodes were then subjected to a battery of electrochemical characterizations, for example, cyclic voltammetry (CV) and galvanostatic charge-discharge (GCD), among others.

Lab 2: XRD patterns were acquired using a diffractometer (Rigaku MiniFlex, Japan) operated with Cu K$_\alpha$ radiation (40 kV and 15 mA) in the 3–65° 2θ range with a step size of 0.04° and a dwell time of 1 s. All XRD patterns were obtained from powders dried overnight at 50 °C in open air.

A SEM (Zeiss Supra 50 VP, Carl Zeiss SMT AG, Oberkochen, Germany) was used to obtain micrographs. The SEM was set in the in-lens detector mode, with a 30-mm aperture, and an accelerating voltage of 3–5 kV.

A VersaProbe 5000 (Physical Electronics, Chanhassen, MN, USA) X-ray photoelectron spectrometer, XPS, was used to obtain XPS spectra. Samples were mounted on the XPS stage using carbon tape. Monochromatic X-rays from an Al-K$_\alpha$ source with a pass energy of 23.5 eV were used to irradiate the sample's surface. Using a spot size of 200 μm, the spectra were acquired by scanning with a step size of 0.05 eV. CasaXPS v.2.3.21PR1.0 software was used for peak fitting and chemical-composition analysis. A Shirley background was used. The spectra were calibrated by setting the C─C peak to 285.0 eV.

The transmission electron microscope, TEM, images, and selected area electron diffraction, SAED, patterns were acquired with a TEM (JEOL 2100F, Tokyo, Japan) equipped with a Schottky field emission electron source. After washing with EtOH until pH is 7, ≈3 μL of the colloid were drop cast onto a carbon-mesh grid sample holder. These specimens were then left to air-dry at RT overnight before imaging them in the TEM.

To explore the liquid crystal domains of our 1DL suspensions, a concentration of 40 g L^{-1}, was diluted to concentrations of 0.1, 1, 10, 15, 20, 28, and 35 g L^{-1}. This dilution process involved adding deionized, DI, water under vigorous stirring. Next, 20 μL of each 1DL suspension was cast onto pre-cleaned glass slides through sonication in anhydrous isopropanol (Sigma Aldrich, ≥99.5%). The thicknesses of the deposited suspension were controlled by employing ≈34 μm-thick polyethylene spacers. Following the deposition, a cover slide was delicately positioned over the 1DL droplet. All solutions were stored in dark ambient environments to avoid evaporation and photodegradation and were degassed by bath-sonication for 2 min before deposition. A polarized light microscope, (PLM) (Olympus BX51) microscope equipped with a digital camera (Diagnostic Instruments SPOT Insight model 3.2.0) was used to image the slides. Subsequent processing of all images was performed using advanced image acquisition software. The polarizer was positioned perpendicular to the analyzer in all acquired images.

The rhodamine 6G, photodegradation was monitored with a UV–vis spectrophotometer (Cary 60, Agilent, Santa Clara, CA, USA) in the 200 to 500 nm range, with a scan rate of 60 nm min^{-1} in quartz cuvettes.

3. Results and Discussion

3.1. Crystallinity

Figure 3A,B plot select XRD patterns of the various reaction products obtained herein. Figure 3A plots the XRD patterns – on a semi-log scale – of samples made in Labs 1 and 2, at R = 0.2, as a function of reaction times at 80 °C. Figure 3B plots the XRD patterns, on a semi-log scale, obtained as a function of R, after reaction at 80 °C for 24 h. From the totality of these results, it is clear that, at least at the XRD level, the reaction product is neither a function of R, reaction time, nor laboratory location. Said otherwise, the reaction product is quite forgiving in terms of R and time.

As noted in the introduction, 1DLs grow in the [100] direction and stack in the [010] direction (Figure 1A).[22] The low-angle peak labeled (020) and its associated d-spacing, $d_{020} = 11.5$ Å, denotes the center-to-center distance between two neighboring 1DLs. The peak at a 2θ of ≈48° is indexed as (200); the peak at 2θ of ≈62° is indexed as a (002) peak. The lattice parameters a, and c calculated from these peaks are Å 3.78 Å and 2.96 Å, respectively. These values are in excellent agreement with our previous 1DL work and, as importantly, previous 2D lepidocrocite work in the literature.[24,26] Table S1 compares the d-spacing obtained herein (first column) with those obtained previously when starting with TiB_2 (last column).[24]

From the XRD patterns, we reach the following conclusions:

1) In all cases, 1DLs are produced. This is an important conclusion because it implies that 1DLs can be made with water-soluble precursors.
2) The locations of the various peaks are independent of reaction times, temperatures or R values (Figure 3A). It follows that the reaction product is a weak function of these factors which bodes well for scaling up.
3) Because previously we did not obtain 1DLs starting with TiO_2 powders, we assumed that part of the transformation required an oxidation step. The results shown here belie this assumption since here the initial Ti oxidation state is 4+.
4) In the FF XRD patterns (linear scale, Figure 3C), the intensities of the 0k0 peaks are significantly stronger than the others. This confirms that the 1DLs stack along the b direction as shown in Figure 1A. It is worth noting that in very dilute colloid suspensions, the 1DLs separate from each other. With increasing concentrations, they start to coalesce, or self-assemble, in the c direction forming quasi-2D layers (Figure 2E) that are normal to the XRD plane.
5) In the TiB_2 case, it is difficult to totally rid the reaction product of TiB_2. Even after 5 d at 80 °C.11 Here no peaks belonging to $TiOSO_4$ were observed (Figure S4, Supporting Information). Since these XRD results were carried out on EtOH washed or FFs after drying it follows that either the $TiOSO_4$ was washed away and/or it is present in an amorphous state. As discussed below, XPS results suggest that it is all washed away.

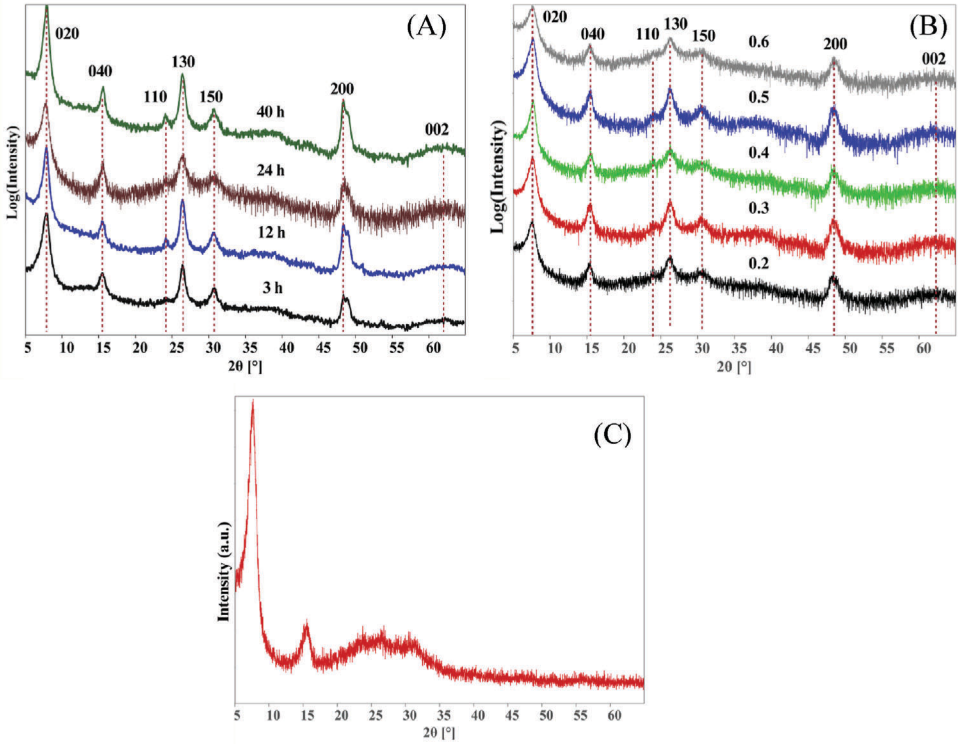

Figure 3. Effects of reaction times and R values at 80 °C, on XRD patterns on a, A) Semi-log scale of PMPs— for samples reacted at times ranging from 3 to 40 h, all at R = 0.2. All samples were washed with ethanol before drying at 50 °C in air overnight, B) Semi-log scale as a function of R indicated on panel, C) Linear scale for FF.

3.2. Morphology and Microstructure

In the introduction, we mentioned that if the reaction product is washed to pH 7 in EtOH and dried, PMPs were obtained. The SEM micrographs, shown in **Figures** 4 and S1 (Supporting Information), demonstrate the same occurs here. The self-assembly of the NFs into PMPs results in free-flowing, non-agglomerated, powders. Figure 4A and Figure S1A (Supporting Information) show good powder dispersions with some aggregation with particle sizes that range widely in size, from submicrometer, to some that are 100 µm in diameter. The latter are probably agglomerates of the finer particles (Figure 4B).

At even higher magnifications (Figure 4C), the PMPs appear to be comprised of wispy/fluffy nanoparticles comprised of small 1DL snippets. The PMPs obtained here are less porous than the ones obtained when TiB_2 is the precursor.[25] It is hereby acknowledged that what determines the particle size distribution, PSD, of the PMPs is unclear at this time. Understanding what affects this distribution, and how to control it, is an important question that is beyond the scope of this work, but one we are currently addressing.

SEM-EDS maps of these particles (Figure S2, Supporting Information) confirm that the only elements present are Ti and O. The same is true of filtered films (Figure S3, Supporting Information). Table S2 (Supporting Information) summarizes the EDS results.

Typical cross-sectional SEM micrographs of FFs are shown in **Figure** 5A to C at different magnifications. The 1DL self-assembly results in planer, 2D-like structures.

To image the 1DLs themselves, the water colloid suspension was diluted to 0.001 gL^{-1} before casting a drop onto a TEM grid mesh. Typical SEM micrographs (**Figure** 6A–D), leave little doubt as to the 1D nature of our material. As the 1DL concentration increases, the "pores" in Figure 6B disappear as more 1DLs are deposited in the same region. The resulting material is thus a q-2D one (Figure 5). The resulting material has an open and disordered appearance that is strikingly similar to a messy spider web (inset in Figure 6C).[32] To further probe the structures obtained, we combined SEM and TEM micrographs of diluted colloids (Figure 6). Figure 6A,B are those of a material reacted for 3 h at 80 °C at two different magnifications. At lower magnification (Figure 6A), here again, the structures are reminiscent of a disordered spider web. They are also reminiscent of cellulose microfibers (inset in 6D).[33]

From the higher magnification SEM micrographs, the smallest 1DL diameters are of the order of 2 nm (inset of Figure 6A). Essentially, the same microstructures were obtained with other colloids. For example, Figure 6C,D shows the 1DLs obtained after reaction at 80 °C for 48 h. The resulting material has an open and disordered appearance that is again strikingly similar to a messy spider web shown in the inset of Figure 6C. The twisting and entwining characteristics of the 1DLs are most obvious in Figure 6D.

Figure 6E shows a typical TEM micrograph, with SAED patterns, of an ordered region. Note that in some locations, amorphous and ordered regions co-exist. This micrograph is identical

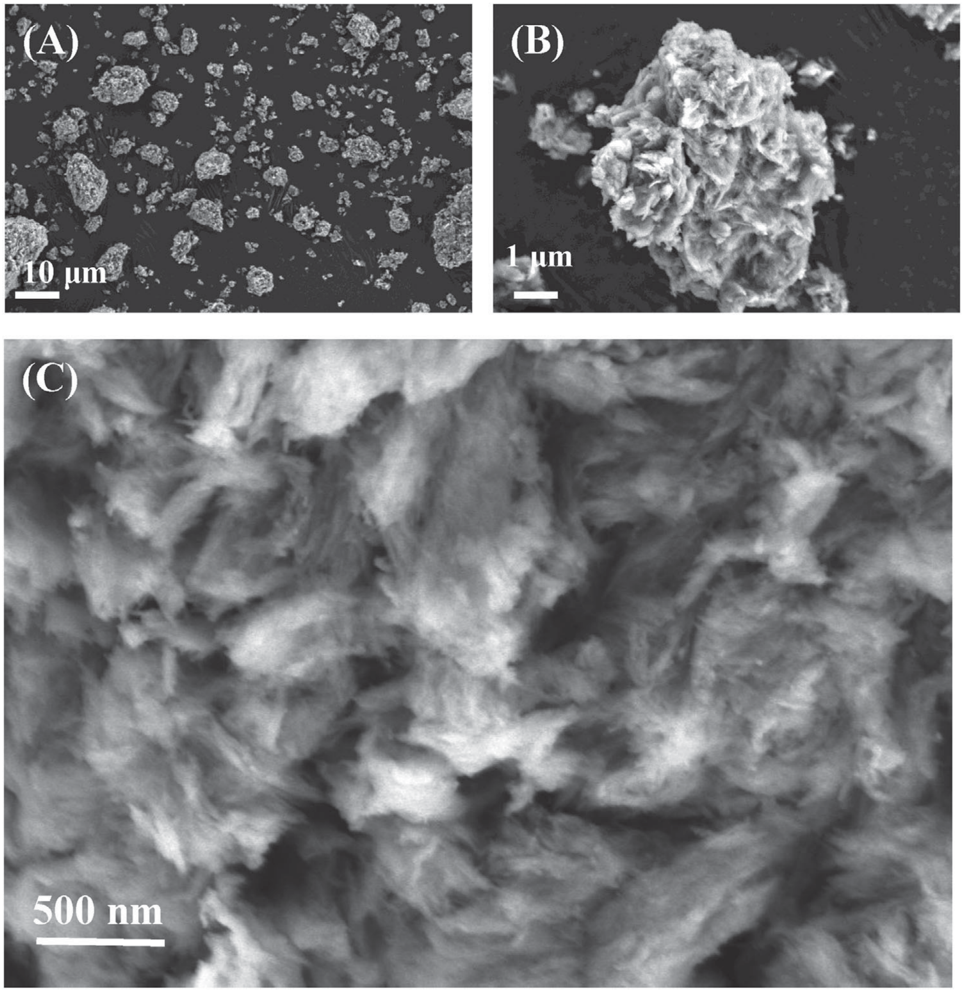

Figure 4. Typical SEM micrographs of PMPs, at A) low, B) intermediate, and C) highest magnification.

to those previously seen.[26] The arcs in the SAED pattern (inset in Figure 6E) are unimpeachable evidence for the 1D character of our materials. The 1DLs grow in the [200] direction and stack the [010]. The results are also consistent with the XRD patterns shown in Figure 2. Figure S5 (Supporting Information) indexes the SAED pattern, including the arcs. The table in Figure S5B (Supporting Information) compares these d-spacings with those obtained from the XRD patterns showing excellent agreement.

As importantly, the results shown in Figure 6B we can now shed light on a paradox encountered in our previous work,[26] namely, that the 2D flakes were TEM amorphous, but still resulted in XRD peaks such as the ones shown in Figure 3. As the q-2D layers thicken by the self-assembly of 1DL, their overlap and twisting (e.g., Figure 6D) results in the extinction of any SAED patterns but *not* XRD peaks.

Table S2 tabulates the EDS results obtained in the SEM, revealing that at 1:1.86 ± 0.15, the Ti:O ratio, respectively, is <2, which is consistent with our previous work.[17] The <2 ratio also confirms that what we produce is not titania, but rather a titanate. At 0.5 wt.%, the sulfur, S, EDS signal was quite low, which serves as a testament to the effectiveness of our post-synthetic purification methods.

To confirm some of these conclusions, we carried out a XPS study on FF, the results of which are shown in **Figure 7**. The C 1s spectrum (Figure 7A) presents a prominent peak at 285 eV that corresponds to the binding energy, BE, typically associated with C atoms in a C—C bond environment. This peak was used for calibration. Adjacent to this are two other peaks that can be attributed to carbon–oxygen (C—O) and carboxyl (C═O or COOH) functional groups, respectively. These peaks suggest a complex chemical environment with multiple carbon-containing species on the surface of the material. This is in complete agreement with our previous 1DL work.[23]

The O 1s spectrum (Figure 7B) displays a pronounced peak observed at a BE of ≈530.0 eV, which is a signature of O atoms in a metal-oxide configuration. The sharp and well-defined nature of this peak points to a consistent and predominant metal-oxide bonding environment, reinforcing the material's oxide character of TiO_2.[34] In the Ti spectrum (Figure 7C), the Ti $2p_{3/2}$ peak, which is the most pronounced in this region located at BE of ≈458.5 eV, is typically indicative of titanium in a Ti(IV) oxidation state, associated with titania. Another peak corresponds to Ti 2p $_{1/2}$ having a BE ≈464.1 eV also exists. These two peaks and their BEs agree with those previously published 1DL spectra.[34]

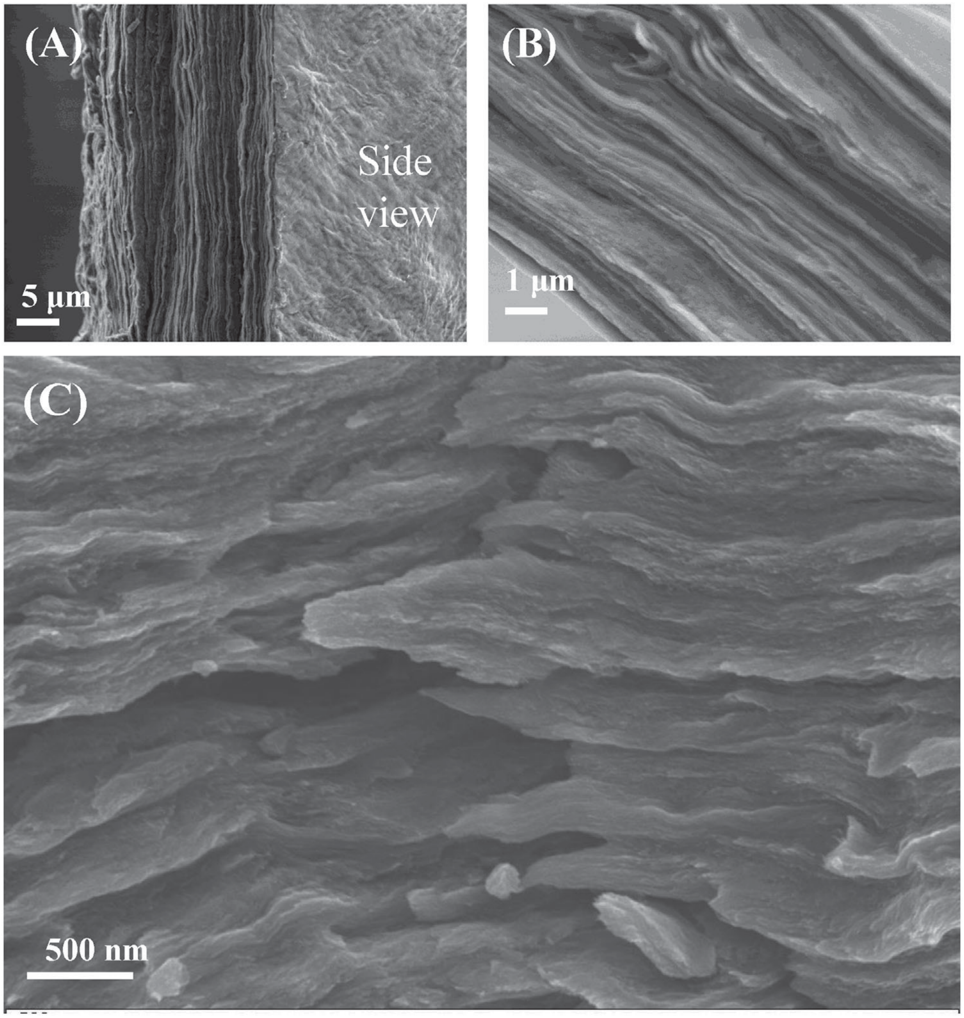

Figure 5. Cross-sectional SEM micrographs of FFs comprised of 1DLs at, A) low B) intermediate, and C) high magnifications.

Consistent with titanate chemistry, at 1:2.4, the oxygen to Ti molar ratio, respectively, obtained from XPS is >2. Why this value is different than the 1.86 value, measured by EDS is unclear at this time, but possibly indicates that the surfaces are more oxygen-rich than the bulk.

Lastly, the S 2p spectrum (Figure 7D) is quite noisy and, if any S is present, it has to be miniscule, confirming the absence of S within the PMPs and is a testament to the efficacy of our washing protocol in riding the 1DLs of S. There was also a small N signal (not shown) that emanates from TMA^+ cations.

3.3. Optical and Electronic Properties

A typical Raman spectrum of q-2D film derived from vacuum filtration of the 1DL colloid (**Figure** 8A) is fully consistent with the lepidocrocite structure.[24,35] For Raman, nine vibrations were detected ≈178, 269, 373, 434, 661, 738, 824, 895, and 931 cm^{-1}, which fairly matches layered lepidocrocite titanates. The Raman bands from 600–940 cm^{-1} are assigned to Ti-O vibrations.[36] Three A_g modes (269, 434, and 824 cm^{-1}) indicate a well-developed layered structure of lepidocrocite.[37]

To measure E_g of our 1DLs, we carried our UV–vis optical absorption measurements in the 200–800 nm wavelength range on 1DLs colloid *and* PMPs. At this juncture, it is not fully clear whether the 1DL bandgap is direct or indirect. DFT calculations for the 2D lepidocrocite in the literature predict a direct bandgap,[5] but most experimental work assumes it is indirect.[23,24] Until this important aspect is clarified, we plot Tauc plots assuming:

$$(\alpha h\nu)^{1/n} = C \times \left(h\nu - E_g\right) \quad (2)$$

where α is the absorption coefficient, $h\nu$ is the photon energy, E_g is the optical bandgap and C is a constant. n = 1/2 or 2 denote direct or indirect bandgap, respectively.[38] **Figure** 9A,B plot the results assuming direct or indirect bandgaps, respectively. A perusal of these results indicates that: i) Not surprisingly, the E_g values obtained depend weakly on whether the material is a direct or indirect semiconductor. ii) For the direct case, (Figure 9A), E_g is ≈3.9 to 4 eV. For the indirect case (Figure 9B), E_g is ≈3.7 eV.

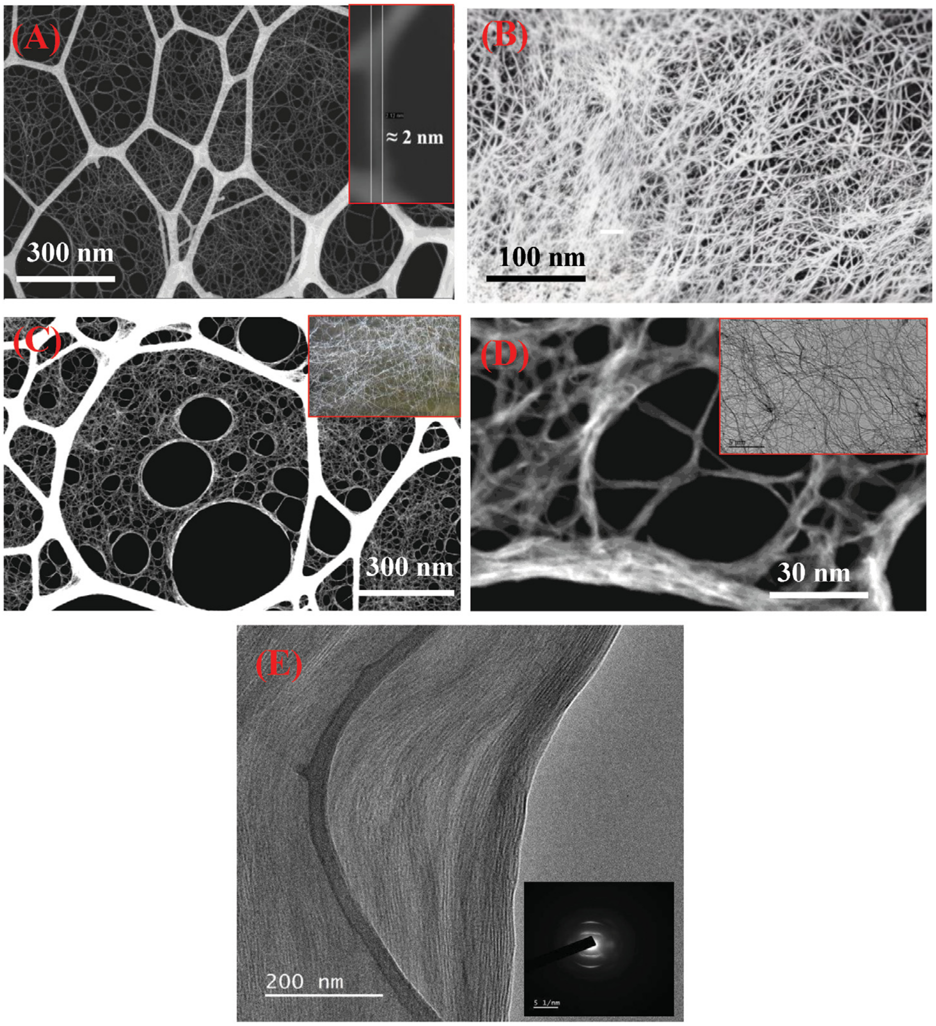

Figure 6. A,B) Typical STEM image of 1DL colloid drop cast on lacey C at different magnifications; the 1DL sample synthesized at 80 °C for 3 h, and Ti/TMAH molar ratio of 0.2. C,D) microstructure of 1DLs synthesized at 80 °C for 48 h, and Ti/TMAH molar ratio of 0.2; (Insets: C) messy spider web, D) Cellulose microfibers). E) The high-resolution TEM images confirm the nano-bundles' uniform assembly along the [200] growth direction and their alignment in the [010] stacking direction, similar to structures observed in TiB2-derived 1DLs. Insets: SAED patterns with clear rings, validating the crystallinity of the 1DLs, which corresponds with XRD findings.

iii) E_g is more or less independent of whether the measurements were carried out on solid PMPs, or 1DL colloidal suspension as shown in red and blue lines in Figure 9, respectively. However, if one makes the reasonable assumption that the E_g values should *not* depend on whether the material is in colloid or solid form, then these results support the direct bandgap assumption. Lastly, the presence of a peak in the Tauc plots for the colloidal suspensions only is quite intriguing. Such a prominent peak has to date not been observed. At this time its origins are unknown. More work, outside the scope of this paper, is needed to understand its origins.

3.4. Electrochemical Properties

The electrochemical behavior of the PMPs derived from $TiOSO_4$ was tested in various aqueous electrolyte media (e.g., acidic: 1 м H_2SO_4, basic: 1 м KOH, and neutral: 1 м Na_2SO_4, 1 м Li_2SO_4). The CV profiles (**Figure 10**A) of the MPPs at varying scan rates (5–100 mVs^{-1}) in 1 м H_2SO_4 exhibit reversible redox peaks, indicating strong faradaic behavior. The electrode delivers a capacity of 55 Fg^{-1} at a 5 mVs^{-1} scan rate in a 1 to – 0.9 V operating window. The GCD (Figure 10D) was performed at various current densities (0.3–3 Ag^{-1}) in the same potential range. Non-linear changes in potential over time imply typical pseudocapacitance caused by reversible redox reactions at the electrode-electrolyte interface. The highest capacity of 19.3 Fg^{-1} was calculated with the specific energy and power of 9 Whkg^{-1} and 261 W kg^{-1}, respectively, at a 0.3 Ag^{-1} current density.

The PMPs in 1 м KOH medium show a broad rectangular CV profile (Figure 10B), indicating a dominating double-layer charge storage in the −1 to 0.5 V potential window. The shape of the voltammogram almost remains consistent throughout the variation in scan rates (5–100 mVs^{-1}), implying good rate

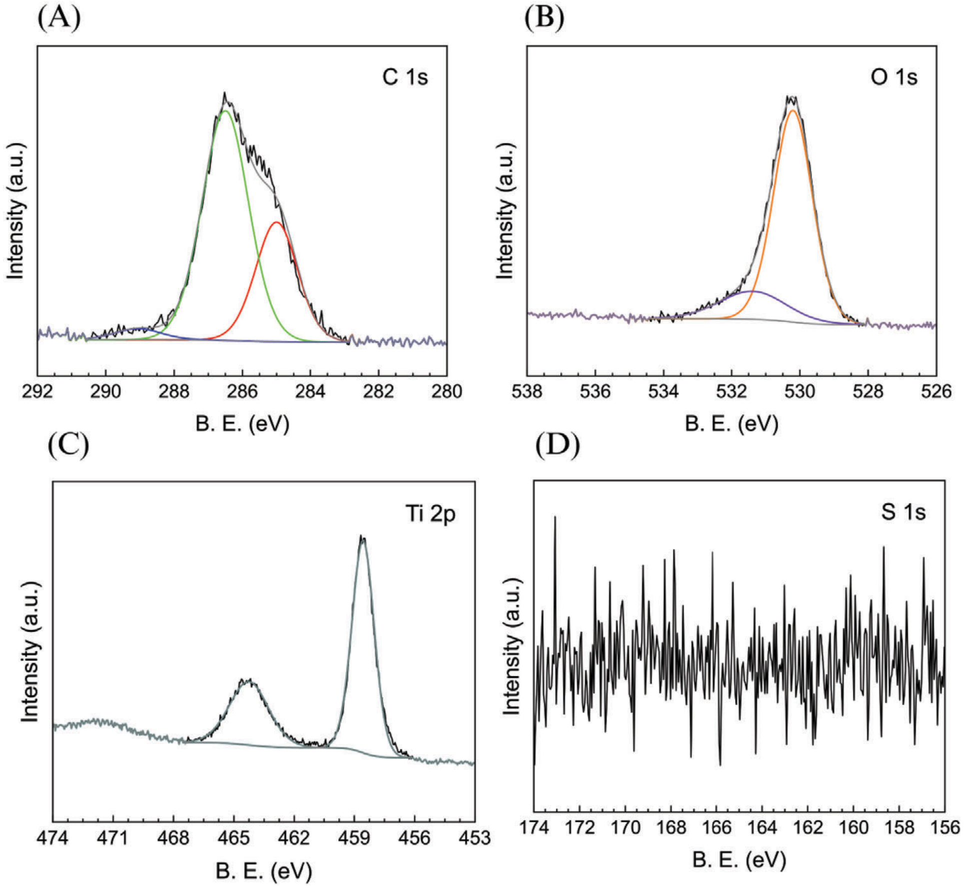

Figure 7. High-resolution XPS spectra of 1DL FF, synthesized at 80 °C for 12 h and R of 0.2, revealing the chemical states and bonding environments of, A) C, B) O, C) Ti, D) S. Spectra demonstrate a clear absence of S.

capability of the electrode. The highest specific capacitance of 3.2 Fg^{-1} was assessed with a specific energy of 1.0 $Whkg^{-1}$. The GCD response (Figure 10E) in the alkaline medium exhibits a linear charge-discharge profile which further confirms the double-layer charge storage at the electrode surface. Figure 10e shows a decrease in coulombic efficiency with decreasing current densities (0.3 Ag^{-1}). The highest specific capacitance of 0.61 Fg^{-1} was calculated with specific energy and power of 0.2 $Whkg^{-1}$ and 210 Wkg^{-1} at a 0.3 Ag^{-1} scan rate.

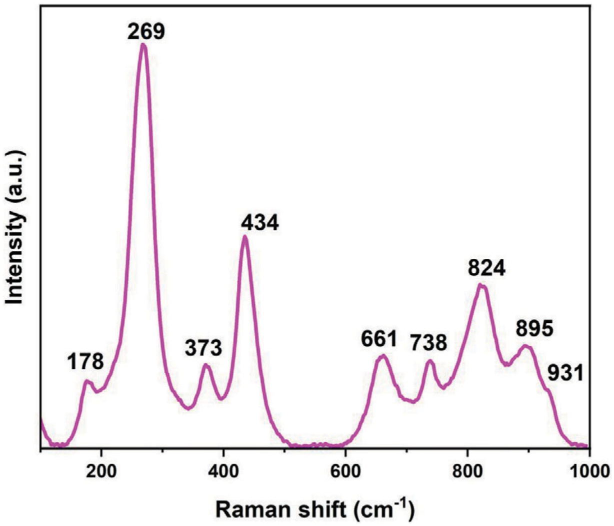

Figure 8. Raman spectra of 2D film comprised of 1DLs. All peaks belong to lepidocrocite.

Figure 10C plots the CV profile of the PMPs in 1 M Na_2SO_4 in a −1 to 1 V potential window. Interestingly, in these neutral aqueous media (Li_2SO_4 and Na_2SO_4), the PMPs show a faradaic charge storage mechanism with a prominent anodic redox peak. The specific capacity of 14 Fg^{-1} with a specific energy of 9 $Whkg^{-1}$ was calculated at a 5 mVs^{-1} scan rate. The GCD was carried out at varying current densities (0.3–3 Ag^{-1}), shown in Figure 10F. The charge-discharge response exhibits a dual charge storage response: a) double-layer charge storage is dominant in the 1 V to -0.5 V potential range, whereas b) pseudocapacitance is observed in the −0.5 to −1 V operating window. The highest specific capacity of 5 Fg^{-1} was calculated at a 0.3 Ag^{-1} current density with specific energy and power of 3 $Whkg^{-1}$ and 300 Wkg^{-1}, respectively.

In the Li_2SO_4 electrolyte (Figure S6, Supporting Information), the PMPs display similar CV and GCD responses as for the Na_2SO_4 medium. The specific capacity from GCD was evaluated at ≈22 Fg^{-1} at a 0.5 current density with specific energy and power of 12 $Whkg^{-1}$ and 214 Wkg^{-1}, respectively. The PMPs show a

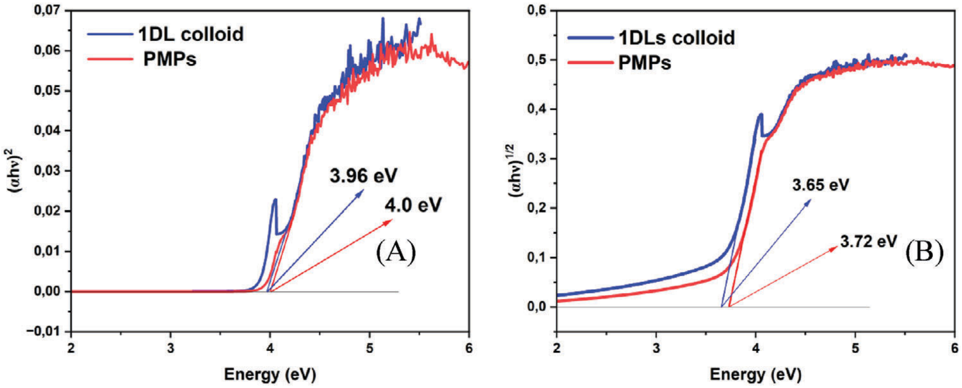

Figure 9. Tauc plots of UV–vis. absorbance spectra of 1DL colloids and PMPs assuming, A) direct, and B) indirect bandgap semiconductors.

wide working potential window and high-power output. Capacitance and energy can be further enhanced through modeling and customization.

To shed some light on what is occurring during cycling, we obtained XRD patterns of the electrodes both before and after conducting the CV tests. The results, shown in Figure S7 (Supporting Information), clearly show the disappearance of the lower angle peak (020) at ≈8° after cycling. It follows that the only information we can glean from these results is that order along the stacking b-direction is lost during cycling. Needless to add more work – beyond the scope of this paper where the emphasis is on processing – is needed to fully understand what is occurring during electrochemical cycling.

3.5. Photocatalytic Properties

In a recent paper, we showed that 1DLs synthesized starting with TiB_2 adsorbed considerable amounts of rhodamine 6G, R6G, and crystal violet, CV, dyes in the dark.[9] At 1850 and 1930 mm kg^{-1}, respectively, these values are higher by a factor of ≈2 than high surface area clays.[9]

When the simulated sun was turned on, the dyes were photochemically degraded even under visible light only. In other words, the dyes sensitized the 1DLs.[9] Typical results obtained previously on TiB_2-derived 1DLs are reproduced in **Figure 11**B, by a lower red curve.[9] We repeated the experiment (R6G dye in a stoichiometric 1:1 ratio with catalyst) with 1DLs synthesized here.

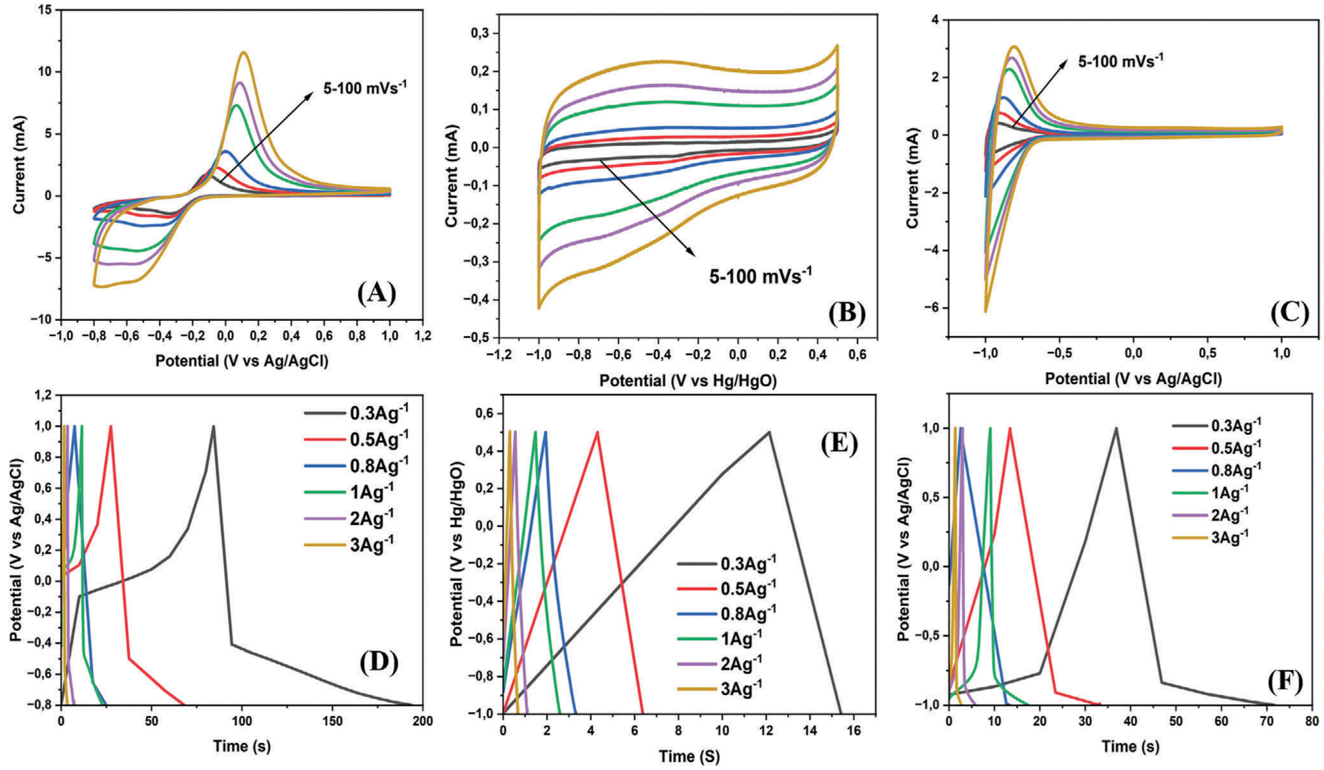

Figure 10. CV curves of the PMPs in (a) 1 M H2SO4, (b) 1 M KOH, (C) 1 M Na2SO4, and GCD curves of the PMPs in (d) 1 M H2SO4, (e) 1 M KOH, (f) 1 M Na2SO4.

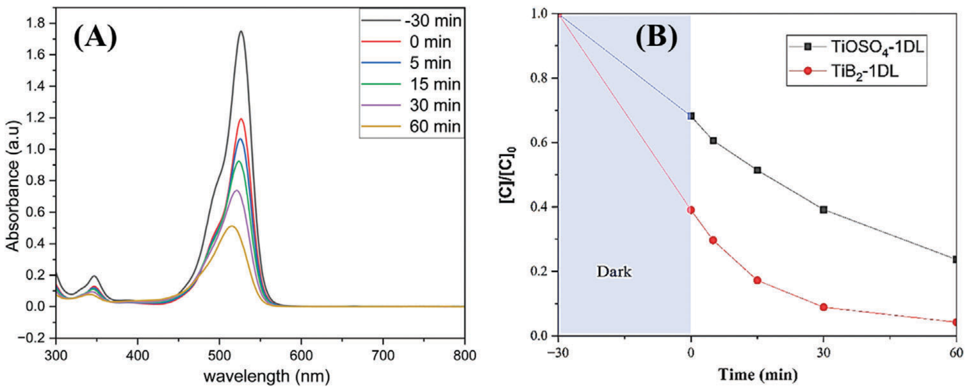

Figure 11. Time dependencies of $TiOSO_4$-1DL synthesized at 80 °C for 12 h at R = 0.2 of, A) UV–vis scans for 1:1 mass ratio 1DL to Rh6G. With time under light, the peak amplitudes drop monotonically, (B) Normalized dye concentration. Red symbols were taken from ref. [26] for colloids made with TiB_2. Labels and graph colors are coordinated.

The time dependence of the absorbance results are plotted in Figure 11A; the changes in concentration with time are plotted in Figure 11B. From these results, it is clear that the 1DLs made here are also photochemically active but adsorb less dye than the TiB_2-based 1DLs in the dark.[9] Why this is the case is unclear at this time. The rates of degradation under light, however, are comparable.

3.6. Liquid Crystals

Figure 12 shows a polarized light microscope, PLM, and micrographs of 1DL aqueous solution at different concentrations at a magnification of 10X. The same results, at a magnification of 20X, can be found in Figure S8 (Supporting Information), and are essentially identical to those at 10X. The isotropic phase is seen when the concentration is <10 gL^{-1}. Stronger birefringence started to appear in samples with concentrations >15 gL^{-1} indicating the formation of liquid crystals. The Sicilian texture is most visible in Figure 12E,F, where the concentrations are 20 and 28 gL^{-1}, respectively indicating a lyotropic nematic phase is formed, similar to our previous observations,[39] and for other 1D nanomaterials.[40–45] In our previous work with TiB_2, the critical concentration was between 1 and 10 gL^{-1}. The higher concentration herein possibly reflects shorter 1DL segments which is consistent with the fact that the colloids are all transparent.

4. Conclusion

Herein we react an inexpensive water-soluble Ti-containing precursor, $TiOSO_4$, with TMAH and convert it into 1DLs with diameters of ≈6 Å. The work shows that the resulting 1DLs chemistries and structures are weak functions of the R values, times – between 3 and 48 h – or temperatures between 60° and 95 °C. Under the conditions tested herein, we can convert 50% of the $TiOSO_4$ in 12 h at 80 °C and 80% at 95 °C. Somewhat surprisingly, there is very little S in our final product. We obtain different morphologies depending on the washing solvent. If only ethanol is used, PMPs form; if water is used, in the last step, quasi-2D flakes

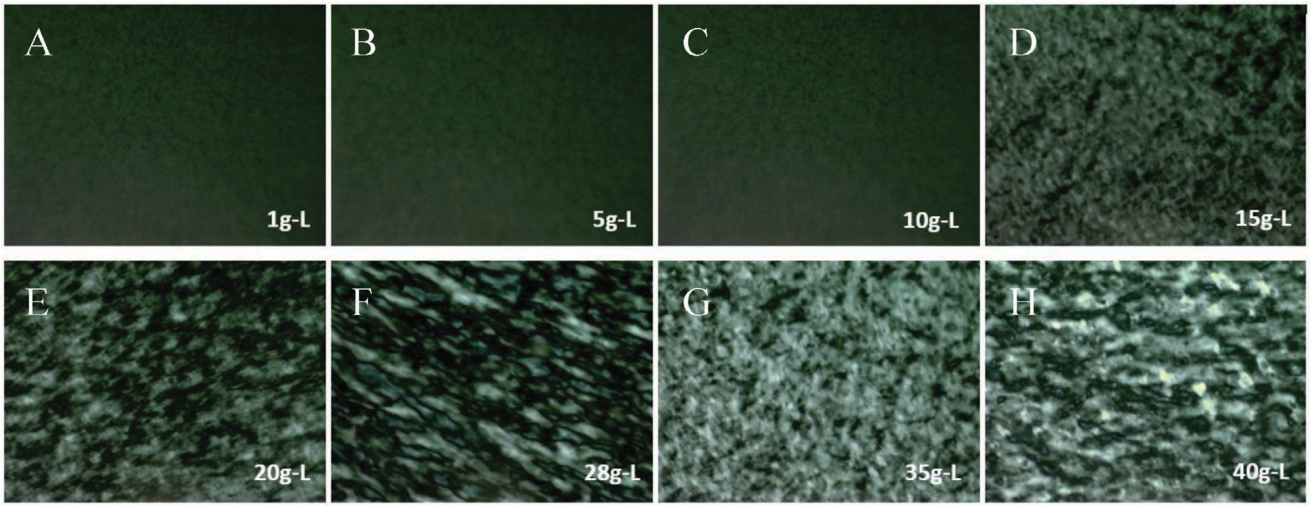

Figure 12. Polarized optical microscope images of colloidal suspensions deposited on a glass slide at 10X. Concentrations are as follows: A) 1, B) 5, C) 10, D) 15, E) 20, F) 28, G) 35 and H) 40 g-L-1.

comprised of 1DLs form instead. Also in agreement with our previous work, E_g is ≈4 eV. Interestingly, the aqueous colloids are, at all concentrations, transparent. This is an intriguing and new result and strongly suggests that the size of the scatterers is much smaller than the wavelengths of visible light, that is, <<200 nm. The 1DLs adsorb R6G in the dark and also degrade them under visible light *only* which implies the dyes sensitize the 1DLs.

The pristine PMPs underwent testing for supercapacitor applications. They exhibited prominent faradaic behavior in acidic and neutral aqueous media, while mostly displaying double-layer behavior in basic medium. PMPs were capable of wide working potential and high power density (300 Wkg^{-1}).

Moreover, the 1DL colloids self-assemble into liquid crystals at concentrations >15 mg mL^{-1}.

In our previous work, we assumed that the precursor had to be insoluble in TMAH and the Ti oxidation state had to be <+4. This work proves that neither is required which is quite important because, i) we can now start with much cheaper precursors and readily, and Scalably, convert them to 1DLs, and ii) increases the precursor chemistries – that are already quite large (>15) in the water-insoluble case – to water-soluble Ti-compounds such as chlorides, sulfates, nitrate, acetates, etc. The commercial/scale-up implications are not insignificant.

Supporting Information

Supporting Information is available from the Wiley Online Library or from the author.

Acknowledgements

The authors acknowledge support from the Knut and Alice Wallenberg (KAW) Foundation for a Scholar Grant (2019.0433) and Project funding (KAW 2020.0033), and from the Swedish Foundation for Strategic Research (SSF) for a Synergy Program (EM16-0004), and European Reaserch Council, European Union (ERC, MULTI2D, 101087713).

Conflict of Interest

The authors declare no conflict of interest.

Data Availability Statement

The data that support the findings of this study are available from the corresponding author upon reasonable request.

Keywords

1D, dye degradation, lepidocrocite titania, Li intercalation, liquid crystals, reaction, sensitization, supercapacitors, tetramethylammonium hydroxide, titanium oxysulphate

Received: November 4, 2024
Published online:

[1] K. Bourikas, C. Kordulis, A. Lycourghiotis, *Chem. Rev.* **2014**, *114*, 9754.
[2] S. G. Kumar, L. G. Devi, *J. Phys. Chem. A* **2011**, *115*, 13211.
[3] W. Fang, M. Xing, J. Zhang, *J. Photochem. Photobiol., C* **2017**, *32*, 21.
[4] L. Wang, T. Sasaki, *Chem. Rev.* **2014**, *114*, 9455.
[5] W. Zhou, N. Umezawa, R. Ma, N. Sakai, Y. Ebina, K. Sano, M. Liu, Y. Ishida, T. Aida, T. Sasaki, *Chem. Mater.* **2018**, *30*, 6449.
[6] D. C. Hurum, A. G. Agrios, K. A. Gray, T. Rajh, M. C. Thurnauer, *J. Phys. Chem. B* **2003**, *107*, 4545.
[7] B. Ohtani, O. O. Prieto-Mahaney, D. Li, R. Abe, *J. Photochem. Photobiol. A: Chem.* **2010**, *216*, 179.
[8] D. M. Tobaldi, R. C. Pullar, M. P. Seabra, J. A. Labrincha, *Mater. Lett.* **2014**, *122*, 345.
[9] A. D. Walter, G. R. Schwenk, J. Cope, K. Sudhakar, M. Q. Hassig, L. Ferrer, A. Mininni, A. J. Lindsay, M. W. Barsoum, *Matter* **2023**, *6*, 4086.
[10] G. Y. Teo, M. P. Ryan, D. J. Riley, *Electrochem. Commun.* **2014**, *47*, 13.
[11] S. Ngamta, N. Boonprakob, N. Wetchakun, K. Ounnunkad, S. Phanichphant, B. Inceesungvorn, *Mater. Lett.* **2013**, *105*, 76.
[12] D. Sofronov, M. Rucki, O. Demidov, A. Doroshenko, E. Sofronova, A. Shaposhnyk, O. Kapustnik, P. Mateychenko, W. Kucharczyk, *J. Mater. Res. Technol.* **2020**, *9*, 12201.
[13] H. Khan, *Reac. Kinet. Mech. Cat.* **2017**, *121*, 811.
[14] H.-J. Hong, G. Ban, S.-M. Lee, I.-S. Park, Y.-J. Lee, *J. Alloys Compd.* **2020**, *844*, 156203.
[15] F. Xiao, K. Tsuru, S. Hayakawa, A. Osaka, *Thin Solid Films* **2003**, *441*, 271.
[16] I. Szilágyi, E. Königsberger, P. M. May, *Inorg. Chem.* **2009**, *48*, 2200.
[17] H. O. Badr, M. W. Barsoum, *Adv. Mater.* **2024**, *36*, 2402012.
[18] K. Kai, Y. Yoshida, H. Kageyama, G. Saito, T. Ishigaki, Y. Furukawa, J. Kawamata, *J. Am. Chem. Soc.* **2008**, *130*, 15938.
[19] H. O. Badr, K. Montazeri, T. El-Melegy, V. Natu, M. Carey, R. Gawas, P. Phan, Q. Qian, C. Y. Li, U. Wiedwald, M. Farle, E. Colin-Ulloa, L. V. Titova, M. Currie, T. Ouisse, M. Barbier, A. Rogalev, F. Wilhelm, M. Hans, J. M. Schneider, C. Tandoc, Y.-J. Hu, J. Snyder, M. W. Barsoum, *Matter* **2022**, *5*, 2365.
[20] A. Zhang, R. Zhao, L. Hu, R. Yang, S. Yao, S. Wang, Z. Yang, Y.-M. Yan, *Adv. Energy Mater.* **2021**, *11*, 2101412.
[21] W. Zheng, J. Halim, L. Yang, H. O. Badr, Z. Sun, P. O. Å. Persson, J. Rosen, M. W. Barsoum, *Batteries Supercaps* **2022**, *5*, 202200151.
[22] K. Sudhakar, T. Kono, T. El-Melegy, H. Badr, P. M. Laxmeesha, K. Montazeri, A. Semisalova, M. Farle, U. Wiedwald, M. W. Barsoum, *J. Magn. Magn. Mater.* **2023**, *582*, 170986.
[23] H. O. Badr, T. El-Melegy, M. Carey, V. Natu, M. Q. Hassig, C. Johnson, Q. Qian, C. Y. Li, K. Kushnir, E. Colin-Ulloa, L. V. Titova, J. L. Martin, R. L. Grimm, R. Pai, V. Kalra, A. Karmakar, A. Ruffino, S. Masiuk, K. Liang, M. Naguib, O. Wilson, A. Magenau, K. Montazeri, Y. Zhu, H. Cheng, T. Torita, M. Koyanagi, A. Yanagimachi, T. Ouisse, M. Barbier, et al., *Mater. Today* **2022**, *54*, 8.
[24] H. O. Badr, F. Lagunas, D. E. Autrey, J. Cope, T. Kono, T. Torita, R. F. Klie, Y.-J. Hu, M. W. Barsoum, *Matter* **2023**, *6*, 128.
[25] H. O. Badr, J. Cope, T. Kono, T. Torita, F. Lagunas, E. Castiel, R. F. Klie, M. W. Barsoum, *Matter* **2023**, *6*, 3538.
[26] K. Sudhakar, A. Karmakar, H. O. Badr, T. El-Melegy, M. Q. Hassig, M. Carey, S. Masiuk, L. Wu, Q. Qian, T. Kono, C. Y. Li, M. W. Barsoum, *Matter* **2023**, *6*, 2834.
[27] N. A. Cardoza, H. O. Badr, R. Pereira, M. W. Barsoum, V. Kalra, *ACS Appl. Mater. Interfaces* **2023**, *15*, 50973.
[28] M. Ge, C. Cao, J. Huang, S. Li, Z. Chen, K.-Q. Zhang, S. S. Al-Deyab, Y. Lai, *J. Mater. Chem. A* **2016**, *4*, 6772.
[29] Y. Habibi, L. A. Lucia, O. J. Rojas, *Chem. Rev.* **2010**, *110*, 3479.
[30] H. O. Badr, V. Natu, S. Neatu, F. Neatu, A. Kuncser, A. M. Rostas, M. Racey, M. W. Barsoum, M. Florea, *Matter* **2023**, *6*, 2853.

[31] L. Wang, H. O. Badr, Y. Yang, J. H. Cope, E. Ma, J. Ouyang, L. Yuan, Z. Li, Z. Liu, M. W. Barsoum, W. Shi, *Chem. Eng. J.* **2023**, *474*, 145635.

[32] B. Vanthournout, *Messy webs – SpiderSpotter*.

[33] BC Cellulose NanoCrystals (CNC/NCC), Cellulose Nanofibrils (CNF), and Bacterial Cellulose (BC).

[34] B. Bharti, S. Kumar, H.-N. Lee, R. Kumar, *Sci. Rep.* **2016**, *6*, 32355.

[35] W. Hu, L. Li, G. Li, Y. Liu, R. L. Withers, *Sci. Rep.* **2014**, *4*, 6582.

[36] T. Gao, P. Norby, H. Okamoto, H. Fjellvåg, *Inorg. Chem.* **2009**, *48*, 9409.

[37] T. Gao, H. Fjellvåg, P. Norby, *J. Phys. Chem. B* **2008**, *112*, 9400.

[38] M. Saadati, O. Akhavan, H. Fazli, *Catalysts* **2021**, *11*, 1445.

[39] T. Zhang, S. Yu, Y. Wu, M. A. Ibrahim, A. D. Walter, G. Schwenk, Y.-J. Hu, M. W. Barsoum, *Matter* **2024**, *7*, 3422.

[40] L.-S. Li, A. p. Alivisatos, *Adv. Mater.* **2003**, *15*, 408.

[41] J. Lagerwall, G. Scalia, M. Haluska, U. Dettlaff-Weglikowska, S. Roth, F. Giesselmann, *Adv. Mater.* **2007**, *19*, 359.

[42] S. Zhang, S. Kumar, *Small* **2008**, *4*, 1270.

[43] S. Zhang, C. I. Pelligra, G. Keskar, P. W. Majewski, F. Ren, L. D. Pfefferle, C. O. Osuji, *ACS Nano* **2011**, *5*, 8357.

[44] S. Umadevi, X. Feng, T. Hegmann, *Adv. Funct. Mater.* **2013**, *23*, 1393.

[45] I. Dierking, S. Al-Zangana, *Nanomaterials* **2017**, *7*, 305.